Materials Letters 344 (2023) 134425

Contents lists available at ScienceDirect

Materials Letters

journal homepage: www.elsevier.com/locate/matlet

Self-powered $In_2Se_3/PtSe_2$ photodetector with broadband and fast response

Haozhe Li [a], Jian Yuan [a,b,c,*], Qinzhuang Liu [a], Haoran Mu [b]

[a] School of Physics and Electronic Information, Huaibei Normal University, Huaibei 235000, Anhui, PR China
[b] Songshan Lake Materials Laboratory, Dongguan, Guangdong 523808, PR China
[c] State Key Laboratory of Applied Optics, Changchun Institute of Optics, Fine Mechanics and Physics, Chinese Academy of Sciences, Changchun 130033, PR China

ARTICLE INFO

Keywords:
2D materials
Heterojunction
Photodetector
Self-powered

ABSTRACT

The emerging van der Waals semiconductor In_2Se_3 has recently gained great attention in the field of optoelectronics, due to its high optical absorption and direct bandgap. Different types of In_2Se_3 photodetectors have been demonstrated with high responsivity, though the detection speed and wavelength range are limited by the device geometry and its absorption edge. In this paper, we have fabricated an α-$In_2Se_3/PtSe_2$ heterojunction photodetector. Taking advantage of the high mobility and narrow bandgap of $PtSe_2$, a wide wavelength response from 405 to 1550 nm and fast repose speed of ~ 127 μs has been achieved in the heterojunction photodetector. Also, benefiting from the strong built-in electric field between In_2Se_3 and $PtSe_2$, the photodetector can work without any external bias with a responsivity highly at 80 mA/W. This fast self-powered $In_2Se_3/PtSe_2$ photodetector presents an avenue for future low-energy-consumption optoelectronics.

1. Introduction

The emerging two-dimensional (2D) materials with unique electronic and optoelectronic properties have provided photodetectors with more materials alternatives in recent decades [1,10]. Among them, α-In_2Se_3 is one of the most ideally active materials [2]. Till now α-In_2Se_3 based photodetectors have achieved a high photoresponsivity of 98,000 A/W [3]. However, the overall device performances are still limited. The cutoff wavelength of the photodetector is only ~ 890 nm, and the device response speed is typically over 1 s, which hinders the application potential, such as telecommunication, imaging and sensing.

Constructing heterostructures by combining α-In_2Se_3 with other high-quality 2D materials is a promising strategy to achieve broadband photoresponse and high response speed. Nowadays, different heterojunction photodetectors based on α-In_2Se_3 have been studied, could achieve efficient photoresponse and extend the wavelength range to around 1100 nm [4,5]. However, the effective detection in telecommunication bands is still difficult in these near-infrared photodetectors. Besides, the response speed, which is a pivotal parameter for weighting the device performance, is relatively slow in these photodetectors.

In this study, we stacked mechanically exfoliated α-In2Se3 and PtSe2 by a direct transfer technique to fabricate a heterojunction photodetector. PtSe2 belongs the Group-10 transition metal disulfides (TMDs), which is considered a promising member with high carrier mobility, layer-dependent band gap ranging from 1.2 eV (monolayer) to 0.21 eV (bilayer), and a broad absorption spectrum. Formation of novel type I energy band alignment by introducing PtSe2 with α-In2Se3, the device can be operated in a self-driven mode without any external bias with a high responsivity of 0.08 A/W. Furthermore, the narrow bandgap nature of PtSe2 compensate the drawback of α-In2Se3, broadband photoresponse is obtained from 405 nm to 1550 nm. The rise and decay times were only 127 and 104 μs, respectively. The α-In2Se3/PtSe2 photodetector demonstrated a broadband photodetection and fast response performance, which is significant for future high-capacity and low-energy consumption optoelectronics.

2. Experimental section

2.1. Material characterizations

Optical microscope (Nikon, Eclipse L200N), scanning electron microscopy (SEM, Gemini 300) and atomic force microscopy (AFM, Bruker, Dimension Icon) are carried out for the morphology and the thickness of α-In_2Se_3 and $PtSe_2$ nanosheets. The phonon vibration modes and surface potential of the heterostructures were performed by Raman spectroscopy (Lab RAM HR800) and Kelvin probe force microscopy (KPFM, Bruker, Dimension Icon), respectively.

* Corresponding author.
E-mail addresses: jianyuan_cq@126.com (J. Yuan), qzliu@mail.ustc.edu.cn (Q. Liu), muhaoran@sslab.org.cn (H. Mu).

https://doi.org/10.1016/j.matlet.2023.134425
Received 23 February 2023; Received in revised form 4 April 2023; Accepted 20 April 2023
Available online 25 April 2023

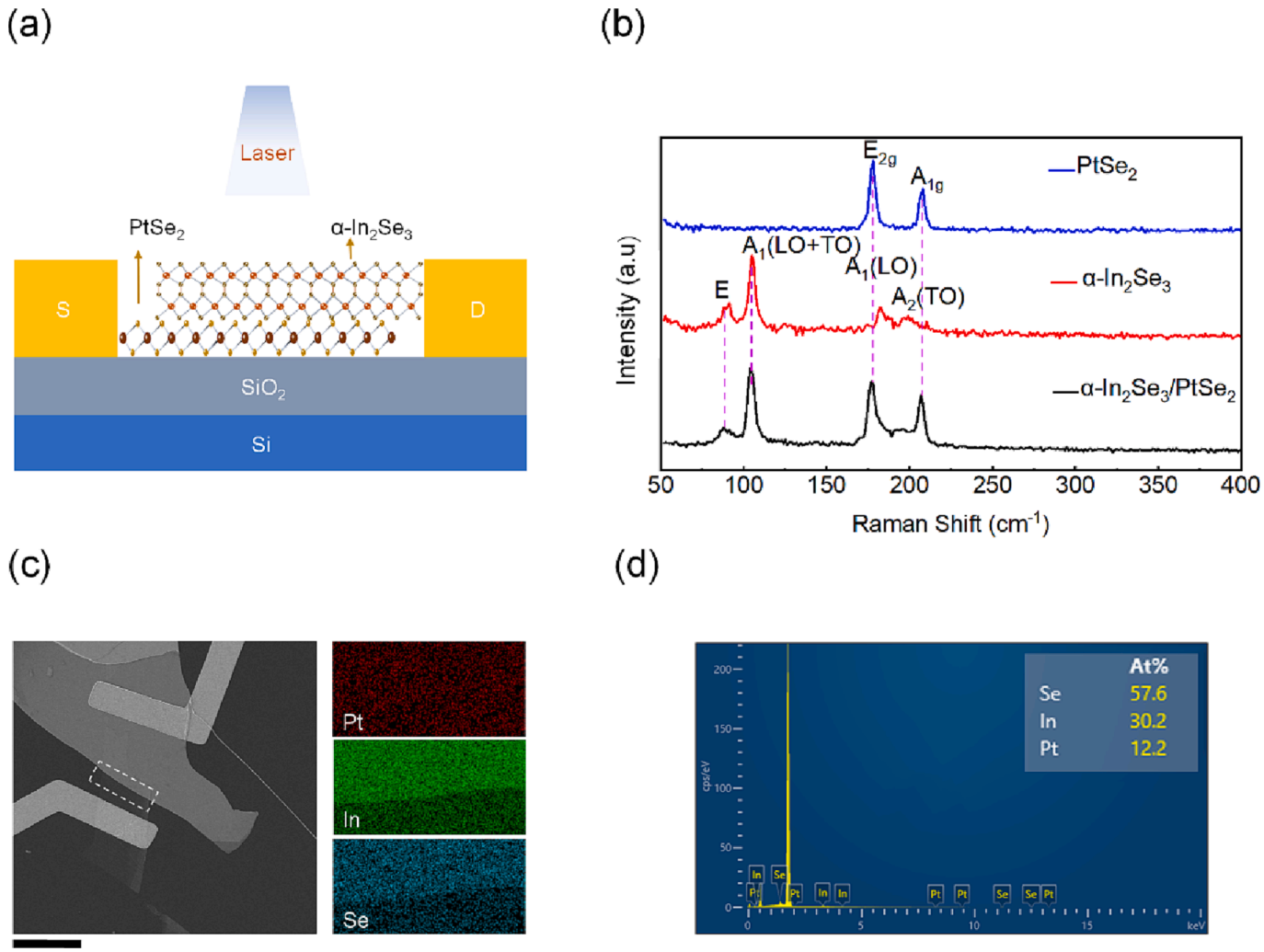

Fig. 1. (a) Schematic diagram of the α-In_2Se_3/$PtSe_2$ heterojunction photodetector. (b) Raman spectra in α-In_2Se_3 (red line), $PtSe_2$ (blue line), and junction (black line) region. (c) SEM image and the associated EDS elemental maps of Pt, In and Se, Scale bar: 25 μm. (d) Energy spectrum intensity.

2.2. Device fabrication and measurements

To create the heterojunction, the $PtSe_2$ layer were first stamped onto the Si/SiO_2 substrate and then heated to 80 °C for 5 min until complete transferred to the substrate. The α-In_2Se_3 sheets were subsequently stamped and stacked on the $PtSe_2$ layer using an optical microscope at the same temperature. The gold electrode with a thickness of 50 nm was deposited using a standard photolithography and sputtering process. Laser diodes of different wavelengths are performed to study the opto-electronic properties of the device.

3. Results and discussion

The structure of our photodetector is shown in Fig. 1a, a 45-nm-thick α-In_2Se_3 stacks on top of a 3-nm-thick $PtSe_2$ flake. From the Raman image in Fig. 1b, all vibrational modes of α-In_2Se_3 and $PtSe_2$ can be observed in the heterojunction region. As can be seen from Fig. 1c, the surface of the junction area of the device is flat and smooth without observable wrinkles and bubbles. According to the EDS results, the selenium and indium elements are densely distributed in the interval of α-In_2Se_3 (in inset of Fig. 1c). As shown in Fig. 1d, the calculated atomic ratio of the elements in the junction region is consistent with the stoichiometric ratio of Pt: In: Se = 1: 2: 5.

A scanning photocurrent system is adopted to study photocurrent generation mechanism of the device. The optical micrograph in Fig. 2a shows the heterojunction region of the photodetector and Fig. 2b is the corresponding mapping result (laser wavelength: 520 nm, zero bias). It is clear that electrons of α-In_2Se_3 and the holes of $PtSe_2$ are driven by the built-in electric field, forming a self-driven photocurrent flowing from the source to the drain.

As shown in Fig. 2c. The contrast between and (Fig. 2c), indicating that the surface potential of the α-In_2Se_3 is much higher than that of $PtSe_2$. Both the contact potential difference (CPD) between the probe and the sample and the difference in the work function between the samples (ΔW) are given by the following equation:

$$e\Delta CPD = \left(W_{probe} - W_{PtSe_2}\right) - \left(W_{probe} - W_{\alpha In_2Se_3}\right)$$

$$\Delta W = W_{PtSe_2} - W_{\alpha In_2Se_3} = -e\Delta CPD$$

where difference of the work functions is about 0.11 eV, as shown in Fig. 2d. Combined with the previously reported work [6], the energy band structure of the device before and after contact can be derived in Fig. 2e and f. The bandgap of $PtSe_2$ with a thickness of 3 nm is about 0.21 eV and that of α-In_2Se_3 is about 1.46 eV. After contact, a type I heterojunction is formed due to the energy offset. At the interface, a built-in electric field is formed from α-In_2Se_3 to $PtSe_2$, consistent with the results obtained in Fig. 2b. When reaching the equilibrium state, the final energy band structure settled as shown in Fig. 2f. Driven by the built-in electric field, the photogenerated electrons in the α-In_2Se_3 migrate to the source, while the holes of α-In_2Se_3 cannot flow through

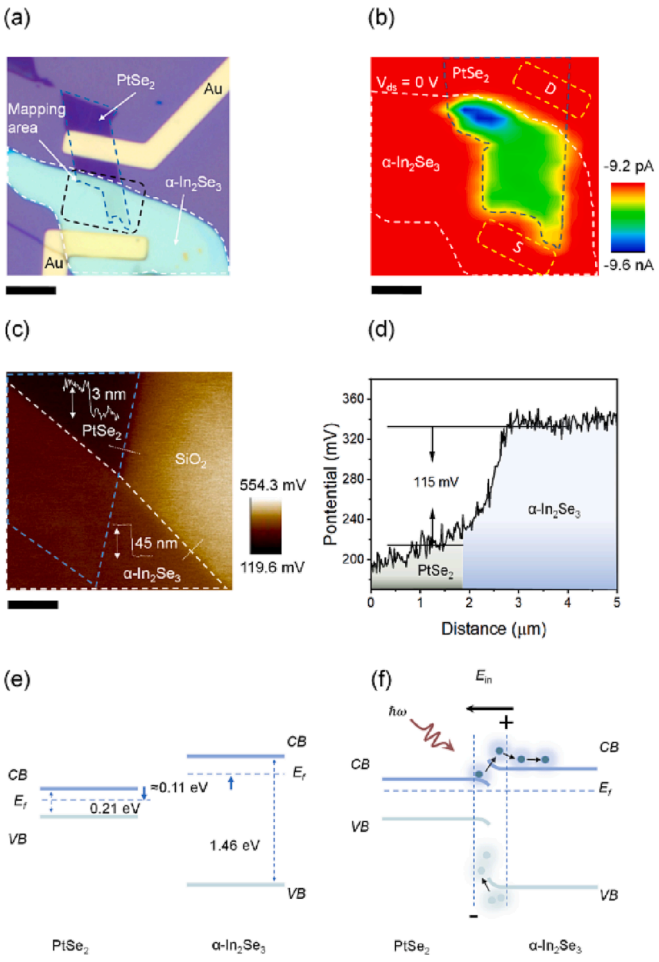

Fig. 2. Photocurrent mechanism study. (a) Optical image. Scale bars: 14 μm. (b) Photocurrent mapping image at 638 nm (V_{ds} = 0 V). Scale bar: 7 μm. (c) KPFM image. Scale bar: 2 μm. (d) CPD between $PtSe_2$ and In_2Se_3. (e) and (f) Energy band alignment before (e) and after contact (f).

the high potential barrier at the interface. The special type-I alignment greatly inhibits the hole diffusion from α-In_2Se_3 to $PtSe_2$ and promotes the carriers' separation, which may lead to a low dark current and high gain. Considering the advantages of high absorption of α-In_2Se_3 and high mobility and wide response of $PtSe_2$, the heterojunction device can realize high-sensitive, broadband, and fast photodetection under self-driven mode.

Then, we investigate the photodetection performance under various light irradiation. The I-V curves in darkness and light are in Fig. 3a and the slope changes with the increasing power. The change in photocurrent is more pronounced under the negative bias, which is due to the fact that the direction of current flow at this time matches the direction of the built-in electric field. The I-V curve near 0 V was presented in the inset of Fig. 3a, where a photovoltaic behavior can be observed. Then the I-T curves are performed at 0 V, giving a high ON/OFF ratio of about 10^3. A photocurrent close to 0.1nA was obtained under a weak light excitation of 0.5 nW, where R and D* are calculated to be 0.08 A/W and 5×10^{11} Jones, respectively, showing high sensitivity. According to Fig. 3c, broadband response has been clearly observed from 638 nm to 1550 nm. The rise and fall time are 127 and 104 μs, respectively (Fig. 3d), where the excitation wavelength is 638 nm and the spot diameter of the laser is 2 μm. By illuminating at a fixed laser power of 10 nW over 1500 s, the photocurrent floating range is about 7.7%, showing the high stability of the devices (Fig. 3e). The detailed optical switching characteristics are shown in Fig. 3f. A comparative study of the key parameters of different In_2Se_3-based photodetectors is summarized in Table 1.

4. Conclusion

In this work, we systematically present the optoelectronic properties of the fabricated α-In_2Se_3/$PtSe_2$ device and reveal the self-driven operation mechanism under the type I energy band arrangement. The device has a responsiveness of 0.08 A/W and a detectivity of 5×10^{11}Jones. The rise time is 127 μs and the fall time is 104 μs, which are more than 100 times shorter than that reported in the previous pure α-In_2Se_3 photodetectors. A broadband response covers from 405 nm to 1550 nm. The stable and reproducible I_{light}/I_{dark} ratio of about 10^3 is obtained over continually operating 1500 s showing the excellent stability, especially the stability of the photo/dark current, which is not shown by the previous α-In_2Se_3 and its heterojunction photodetectors. The Type-I In_2Se_3/$PtSe_2$ heterojunction has a potential for future photodetectors that require high sensitivity and operate in complex identification environments.

Data availability

The authors declare that data has not been used.

CRediT authorship contribution statement

Haozhe Li: Writing – original draft. **Jian Yuan:** Conceptualization. **Qinzhuang Liu:** Conceptualization, Investigation. **Haoran Mu:** Writing – review & editing, Supervision.

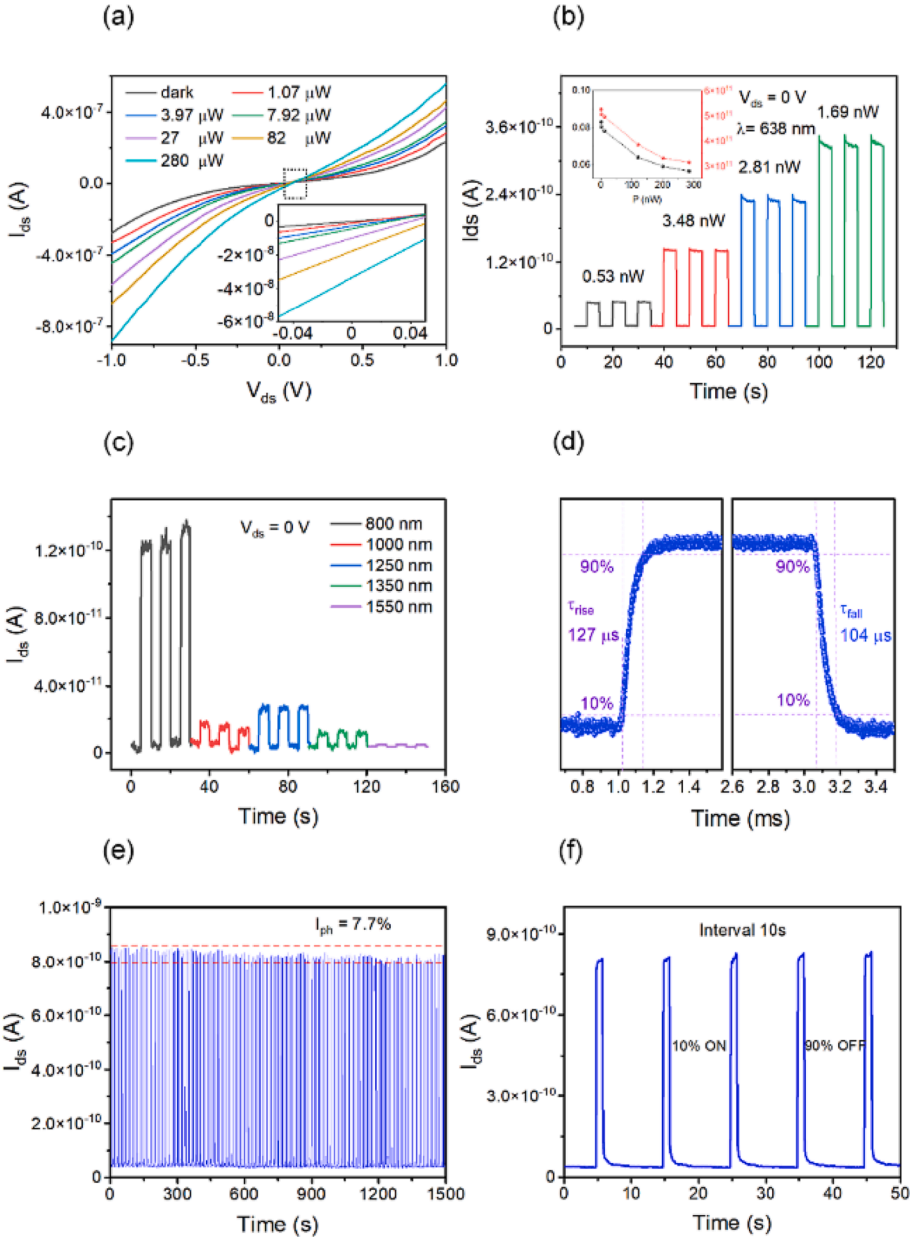

Fig. 3. Photoresponse performance at self-driven mode. (a) I-V curves, where the inset is amplified I-V curves near 0 V. (b) I-T curves, where the inset is R and D* values at 0 V bias. (c) Broadband photoresponse characteristics. (d) rise and fall time. (e) long-term stability measurement. (f) The photo-switching characteristics.

Table 1
Comparison table of important performance parameters of photodetectors.

Materials	External voltage (V)	λ (nm)	R (A/W)	D* (Jones)	Response time	Ref.
α-In_2Se_3/$PtSe_2$	V_{ds} = 0 V	405–1550	0.08	5 × 10^{11}	127/104 μs	This work
α-In_2Se_3	V_{ds} = 1 V	300–1000	720	2 × 10^{12}	1.6 s	[8]
α-In_2Se_3	V_{ds} = 0.3 V, V_g = 45 V	700	1081	1 × 10^{11}	8 ms	[9]
α-In_2Se_3	V_{ds} = 0.3 V, V_g = 45 V	405–940	98,000	3 × 10^{13}	9000 ms	[3]
α-In_2Se_3/WSe_2	V_{ds} = -3 V	400–1100	72	1 × 10^{12}	1.5 ms	[7]
α-In_2Se_3/P-GaN	V_{ds} = -3 V	365–900	0.08	3 × 10^{10}	200 ms	[6]

Declaration of Competing Interest

The authors declare that they have no known competing financial interests or personal relationships that could have appeared to influence the work reported in this paper.

Acknowledgements

This work was funded by the State Key Laboratory of applied optics (SKLAO2022001A13), This work was partially supported by Natural Science Foundation of China (51402120 and 11974127); the Natural Science Foundation of Anhui Province (No. 2008085MA19 and 2008085QF319), Natural Science Foundation of Anhui Higher Education Institutions of China (KJ2014A222, KJ2019ZD40, 2022AH050379 and KJ2020A0047).

References

[1] M. Amani, C. Tan, et al., ACS Nano 12 (7) (2018) 7253–7263.
[2] P.K. Mohapatra, K. Ranganathan, et al., Appl. Mater. Today 20 (2020), 100734.
[3] J.O. Island, S.I. Blanter, et al., Nano Lett. 15 (12) (2015) 7853–7858.
[4] F. Xue, W. Hu, et al., Adv. Funct. Mater. 28 (50) (2018) 1803738.
[5] Y. Chen, X. Yang, et al., Nano Res. 15 (4) (2021) 3711–3719.
[6] S.V. Solanke, R. Soman, et al., SNA 317 (2021), 112455.
[7] H.J. Jin, C. Park, et al., Adv. Mater. Technol. 6 (11) (2021) 6–11.
[8] M. Anandan, H.F. Hsieh, et al., Nanotechnology 31 (46) (2020) 31–46.
[9] B. Tang, L.F. Hou, et al., Nanoscale 11 (27) (2019) 12817–12828.
[10] R. Zhuang, S. Cai, et al.,Nat. Commun 14 (1) (2023) 1621.